Polymer 51 (2010) 1042–1055

Contents lists available at ScienceDirect

Polymer

journal homepage: www.elsevier.com/locate/polymer

Double-brush Langmuir–Blodgett monolayers of α-helical diblock copolypeptides

Le-Thu T. Nguyen [a], Eltjo J. Vorenkamp [a], Christophe J.M. Daumont [b], Gerrit ten Brinke [a], Arend J. Schouten [a,*]

[a] Department of Polymer Chemistry, Zernike Institute for Advanced Materials, University of Groningen, Nijenborgh 4, 9747 AG Groningen, The Netherlands
[b] Department of Solid State Chemistry, Zernike Institute for Advanced Materials, University of Groningen, Nijenborgh 4, 9747 AG Groningen, The Netherlands

ARTICLE INFO

Article history:
Received 20 October 2009
Accepted 5 January 2010
Available online 14 January 2010

Keywords:
α-Helical amphiphilic diblock copolypeptide
Double-brush
Langmuir–Blodgett monolayers

ABSTRACT

The synthesis of amphiphilic diblock copolypeptides consisting of poly(α-L-glutamic acid) (PLGA) and poly(γ-methyl-L-glutamate-*ran*-γ-stearyl-L-glutamate) with 30 mol % of stearyl substituents (PMLGSLG) and their monolayer behavior at the air–water interface have been studied. PLGA-*b*-PMLGSLG was synthesized via a diblock copolymer precursor consisting of poly(γ-*tert*-butyl-L-glutamate) (PtBuLG) and PMLGSLG blocks, with the *tert*-butyl group as a mild acid-labile protecting group for the carboxylic acid. The polymerization conditions were found to influence the α-helix to β-sheet content ratio and can be tuned to significantly enhance the diblock copolypeptide helicity. Purely α-helical PtBuLG-*b*-PMLGSLG diblock copolymers were successfully prepared. After removal of the *tert*-butyl group, the study of the PLGA-*b*-PMLGSLG amphiphilic diblock copolymers in Langmuir monolayers and Langmuir–Blodgett films demonstrated the formation of a stable α-helical double-brush structure, with the helices tilted away from the substrate surface. These double-brush monolayers combine the unique properties arising from the unidirectionally aligned helix macrodipole and the liquid-like features of the side chain mantle of the PMLGSLG block. Such systems are promising for thin film applications requiring incorporation and orientation of bio- and optical molecules.

1. Introduction

In the past, Langmuir–Blodgett layers of polymers mostly involved the situation where the water surface forced the polymeric chains into a two-dimensional (2-D) random coil conformation, either condensed or expanded, depending on the balance of the interactions between neighboring polymeric segments and water-polymer interactions [1,2]. In some cases, these monolayers can be transferred to substrates, but the 2-D conformations of the polymer molecules are intrinsically unstable in the three-dimensional (3-D) situation on a substrate. However, if the glass transition temperature of the polymer is high enough, this unfavorable situation might persist for longer times. Polymers with a rigid-rod conformation are particularly interesting in this respect as they have no other choice but to orient themselves parallel to the water surface, at least in cases at the water surface, where the adhesive forces exceed the cohesive forces [3,4]. Representatives of this class of molecules are polypeptides and synthetic polypeptides in the α-helical conformation in particular. Many studies have been published revealing a range of interesting properties derived from the specific behavior in the Langmuir–Blodgett process and derived from their specific chemical structure [5–8]. Special effects in the multilayers have been introduced by flow-induced orientation during the transfer process [9,10].

These polypeptides have also been used in surface grafting of polymer brushes [11–14]. Many studies on the properties of these ultra-thin layers have been published revealing the unique properties of these systems [15,16]. However, the disadvantage of the surface grafting process is the difficulty in analyzing the grafted polymers.

One possible way to prepare functional ultra-thin polymer films with controlled directional properties is by combining the Langmuir–Blodgett technique with the unique properties of polymer brushes.

Several polypeptide-based amphiphiles have been explored to achieve a perpendicular and unidirectional orientation of α-helices in polypeptide Langmuir monolayers. Kinoshita and his group [17] studied the orientation of various amphiphilic α-helical peptides at the hexane-water and air-water interfaces. The first reported systems were Langmuir monolayers of the amphiphilic diblock copolymers of poly(γ-methyl-L-glutamate) and polyethyleneglycol (PMG-PEG) [18] at the air–water interface and poly(γ-methyl-L-glutamate) bearing the hydrophilic β-cyclodextrin at the terminal (PMG-CyD) at the hexane-water interface [19]. A vertical helix

* Corresponding author. Tel.: +31 503634513; fax: +31 503634400.
E-mail address: a.j.schouten@rug.nl (A.J. Schouten).

0032-3861/$ – see front matter © 2010 Elsevier Ltd. All rights reserved.
doi:10.1016/j.polymer.2010.01.014

orientation of these systems was suggested by the authors based on the consistency of the surface areas corresponding to the solid-state in the isotherms for the same type of polymers with different helix lengths. Nevertheless, the transferability and stability of helix orientation in the transferred films were not addressed.

The orientation of α-helical poly(L-leucine)-based amphiphiles in Langmuir–Blodgett (LB) monolayers has been reported [20,21]. The helix orientation in these LB films was characterized by Fourier transform infrared reflection absorption spectroscopy (FT-IR/RAS). The helices of poly(L-leucine) having a trimethylammonium head group, though lying flat at the air–water interface, were found to be tilted at the hexane-water interface [20]. The LB monolayer of poly(L-leucine)-*b*-polyethyleneglycol diblock copolymers transferred from the air–water interface [21] was shown to have a helix orientation with a tilt at the interface. Yokoi et al. [22] controlled the helix orientation in the monolayer of a diblock copolypeptide consisting of poly(ε-benzyloxycarbonyl L-lysine) and poly(γ-methyl-L-glutamate-L-glutamic acid) at the air–water interface by manipulating the secondary structure of the hydrophilic segment by varying the subphase pH. However, the transferred monolayers contained an amount of β-sheet and random coil structures. Thus the helix tilt angle, estimated to be smaller than 72°, was not calculated.

Niwa et al. [23] and Higashi et al. [24] reported on the orientation of amphiphiles consisting of poly(γ-benzyl-L-glutamate) (PBLG) using FT-IR/RAS. Niwa et al. [23] prepared an α-helix bundle structure by inducing helix association via ionic complexation of a quaternary ammonium-terminated PBLG (PBLG-N^+) with the sulfonate groups of bathophenanthroline disulfonate (BPS) and Fe-BPS. The helix orientation was manipulated by different complexation conditions. The monolayers of the PBLG-N^+ ion complexes, which were prepared in solution, exhibited a tilted helix orientation with a tilt angle of 41°. By performing the complexation between PBLG-N^+ and BPS at the water interface, the average helix tilt angle was decreased to 25°. A perpendicular helix orientation was claimed when PBLG-N^+/BPS was complexed with Fe-BPS dispersed in the water subphase.

Higashi et al. [24] reported the formation of a stable Langmuir monolayer of an amphiphilic diblock copolymer of PBLG and poly(L-glutamic acid) (PLGA) and transfer of the monolayer onto a hydrophobized substrate. The system was suitable for the enantiomeric capture of α-amino acids in aqueous solution by the PLGA segments. The tilt of helices in the transferred monolayers was found to vary with the transfer surface pressure and an average helix tilt angle of 33–45° was obtained at a range of pressures of 20–40 mN/m.

The purpose of the present study is to fabricate monolayers with unidirectionally aligned α-helices of poly(γ-methyl-L-glutamate-*ran*-γ-stearyl-L-glutamate) with 30 mol % of stearyl substituents (PMLGSLG). The hydrophobic PMLGSLG with its hairy-rod structure provides stable LB films with a highly ordered array of α-helices aligned parallel to the substrate, with the flexible stearyl side chains acting as an oily mantle for the rigid rods [9]. Hairy-rod polyglutamates show lyotropic and thermotropic behavior [25,26] and have received considerable attention in the past years [10,27–40]. Besides the rigid-rod feature, the liquid-like properties of the surrounding amorphous side chains make PMLGSLG attractive as matrices for embedding and orienting dyes [41], transporting charge carriers in photoconductive devices [42] as well as optical recording and storage materials [43,44]. Therefore, monolayers with unidirectional helix orientation of PMLGSLG have potential as functional polar ordered thin films for incorporating and orienting optical molecules, and for stabilizing biomolecules. To induce the helix orientation of the PMLGSLG rods at the interface we studied diblock copolymers of PMLGSLG and poly(L-glutamic acid) (PLGA), since PLGA as the hydrophilic block has been demonstrated for the PBLG–PLGA diblock copolymer by Higashi et al. [24] to be well-oriented in the water subphase with a stable secondary structure. This paper reports on the preparation of the amphiphilic PLGA-*b*-PMLGSLG diblock copolymers in the α-helical structure and their monolayer behavior at the air–water interface.

2. Experimental section

2.1. Materials

N-(*tert*-butoxycarbonyl)-L-glutamic acid γ-*tert*-butyl ester (Boc-Glu(OtBu)-OH) (Fluka, 99%), α-pinene (Aldrich, 98%), triphosgene (Aldrich, 98%), *n*-hexylamine (Fluka, 98%) and trifluoroacetic acid (TFA) (Merck, 99%) were used as received. γ-Methyl L-glutamate (Aldrich, 99%) was recrystallized from ethanol (70%) before use. γ-Stearyl L-glutamate was synthesized according to the procedure described by Wassermann et al. [45]. All solvents used for synthesis were dried and distilled before use according to standard procedures.

2.2. γ-Methyl and γ-stearyl L-glutamate N-carboxyanhydrides (MLG-NCA and SLG-NCA)

MLG-NCA and SLG-NCA were synthesized following the method described by Cornille et al. [46] with some minor modifications, namely triphosgene was employed as a phosgene source and *n*-hexane was used in the precipitation and washing process. MLG-NCA: Yield: 83%. ^{1}H NMR (300 MHz, $CDCl_3$): δ 2.06–2.34 (m, 2H, β-CH_2), 2.57 (t, 2H, γ-CH_2), 3.72 (s, 3H, OCH_3), 4.40 (t, 1H, α-CH), 6.38 (s, 1H, NH). IR (ATR, cm^{-1}): 3304 (ν N–H), 2957 (ν_a CH_3), 2906 (ν_a CH_2), 2864 (ν_s CH_2), 1861 (ν C=O anhydride), 1780 (ν C=O anhydride), 1709 (ν C=O ester). SLG-NCA: Yield: 81%. ^{1}H NMR (300 MHz, $CDCl_3$): δ 0.88 (t, 3H, CH_3), 1.25 (s, 30H, OCH_2CH_2-$(CH_2)_{15}$), 1.63 (t, 2H, OCH_2-CH_2), 2.06–2.33 (m, 2H, β-CH_2), 2.56 (t, 2H, γ-CH_2), 4.10 (t, 2H, OCH_2), 4.38 (t, 1H, α-CH), 6.14 (s, 1H, NH). IR (ATR, cm^{-1}): 3261 (ν N–H), 2919 (ν_a CH_2), 2849 (ν_s CH_2), 1856 (ν C=O anhydride), 1790 (ν C=O anhydride), 1732 (ν C=O ester).

2.3. γ-Tert-butyl L-glutamate N-carboxyanhydrides (tBuLG-NCA)

tBuLG-NCA was prepared employing the method described by Wilder et al. [47]. A modification based on the procedure of Cornille et al. [46] was applied, in which α-pinene was used instead of triethylamine as an HCl capturing agent. All of the reaction, washing and purification steps were carried out under dry nitrogen. A mixture of 6.0 g (19.8 mmol) of Boc-Glu(OtBu)-OH, 7 mL (6 g, 44 mmol) of α-pinene and 70 mL of ethyl acetate was heated to 65 °C and stirred for 20–30 min. After an addition of 4.0 g of triphosgene (13.5 mmol), the reaction mixture was stirred at the same temperature for 24 h. The completion of the reaction was determined by ^{1}H NMR (complete disappearance of δ 5.19–5.27 (d, NH) and 4.20–4.36 (α-CH) ppm). After evaporation of the solvent, the product was recrystallized three times from 40 mL of CH_2Cl_2/*n*-hexane (1:3, v/v). The obtained white product was dried under vacuum and stored under nitrogen at −18 °C. Yield: 78%. ^{1}H NMR (300 MHz, $CDCl_3$): δ 1.45 (s, 9H, $(CH_3)_3$), 2.01–2.32 (m, 2H, β-CH_2), 2.47 (t, 2H, γ-CH_2), 4.37 (t, 1H, α-CH), 6.46 (s, 1H, NH). IR (ATR, cm^{-1}): 3350 (ν N–H), 2985 (ν_a CH_3), 2935 (ν_a CH_2), 2869 (ν_s CH_2), 1859 (ν C=O anhydride), 1790 (ν C=O anhydride), 1728 (ν C=O ester).

2.4. Synthesis of PtBuLG

PtBuLG (also $(tBuLG)_n$, with DP = n) was synthesized by polymerization of tBuLG-NCA at 0 °C using a primary amine initiator. Typical procedure: In a round-bottom flask capped with a rubber septum and under dry nitrogen, tBuLG-NCA was dissolved in chloroform (0.35 mol L^{-1}). The reaction mixture was cooled to 0 °C and a volume of *n*-hexylamine was injected via a syringe. The reaction mixture was stirred at 0 °C for a week. Then, the reaction solution was poured into a large amount of ethanol and chloroform was removed by rotary evaporation. The polymer precipitate was collected by filtration, washed extensively with cold ethanol, and dried at 50 °C under vacuum. ^{1}H NMR (300 MHz, $CDCl_3$): δ 1.42 (s, 9H, $(CH_3)_3$), 1.92–2.71 (t, 4H, β-CH_2 & γ-CH_2), 4.00 (s, 1H, α-CH), 8.25 (s, 1H, NH). IR (ATR, cm^{-1}): 3287 (amide A), 3060 (amide B), 2978 (ν_a CH_3), 2933 (ν_a CH_2), 2872 (ν_s CH_2), 1724 (ν C=O ester), 1650 (amide I, α-helix), 1544 (amide II, α-helix), 1520 (parallel amide II, α-helix, visible as a shoulder), 1367 (δ_s CH_3).

2.5. Synthesis of PMLGSLG (also $(MLGSLG)_n$, with DP = n)

In a round-bottom flask capped with a rubber septum and under dry nitrogen, MLG-NCA and SLG-NCA (70:30, mole ratio) were dissolved in the solvent. A volume of triethylamine used as initiator was injected via a syringe. After 7 days under stirring, the product was precipitated into methanol, filtered and dried under vacuum at 50 °C. ^{1}H NMR (300 MHz, $CDCl_3$ (10% TFA-d1)): δ 0.87 (t, 3H, $O(CH_2)_{17}$-CH_3), 1.25 (s, 30H, OCH_2CH_2-$(CH_2)_{15}$), 1.60 (s, 2H, OCH_2-CH_2), 1.94–2.30 (d, 2H, β-CH_2), 2.5 (s, 2H, γ-CH_2), 3.69 (s, 3H, OCH_3), 4.08 (s, 2H, OCH_2), 4.53 (s, 1H, α-CH), 8.27 (s, 1H, NH). IR (ATR, cm^{-1}): 3284 (amide A), 3068 (amide B), 2954 (ν_a CH_3), 2923 (ν_a CH_2), 2852 (ν_s CH_2), 1734 (ν C=O ester), 1652 (amide I, α-helix), 1548 (amide II, α-helix), 1512 (parallel amide II, α-helix, visible as a shoulder).

2.6. Synthesis of PtBuLG-b-PMLGSLG

Optimal conditions (i.e. conditions giving 100% α-helix content): PtBuLG-*b*-PMLGSLG (also $(tBuLG)_m$-*b*-$(MLGSLG)_n$, with m and n respectively the DPs of the PtBuLG and PMLGSLG blocks) was synthesized by polymerization of MLG-NCA and SLG-NCA (70:30, mole ratio) in chloroform (0.05 mol L^{-1}) at 0 °C using PtBuLG as a macroinitiator (Scheme 1). The polymerization was carried out for a week. The product was collected by dropwise precipitation into methanol. Using a solvent-nonsolvent (chloroform-methanol) volume ratio not lower than 1/10, the unreacted PtBuLG, if any, can be completely eliminated upon precipitation. ^{1}H NMR (300 MHz, $CDCl_3$): δ 0.87 (t, 3H, $O(CH_2)_{17}$-CH_3), 1.25 (s, 30H, OCH_2CH_2-$(CH_2)_{15}$), 1.42 (s, 9H, $OC(CH_3)_3$), 1.61 (s, 2H, OCH_2-CH_2), 1.91–2.78 (t, 4H, β-CH_2 & γ-CH_2), 3.70 (s, 3H, OCH_3), 4.02 (s, 2H, OCH_2), 4.10 (s, 1H, α-CH), 8.27 (s, 1H, NH). IR (ATR, cm^{-1}): 3290 (amide A), 3064 (amide B), 2977 (ν_a CH_3), 2924 (ν_a CH_2), 2853 (ν_s CH_2), 1728 (ν C=O ester), 1649 (amide I, α-helix), 1545 (amide II, α-helix), 1520 (parallel amide II, α-helix, visible as a shoulder), 1367 (δ_s CH_3).

2.7. Removal of the tert-butyl group

PtBuLG-*b*-PMLGSLG was dissolved in TFA (25–30 mg mL^{-1}) and then stirred for 1 h. The resulting PLGA-*b*-PMLGSLG (also $(LGA)_m$-*b*-$(MLGSLG)_n$, with m and n respectively the DPs of the PLGA and PMLGSLG blocks) was precipitated into ether, washed several times with ether and dried under vacuum at 50 °C. ^{1}H NMR (300 MHz, $CDCl_3$/d-TFA (2/1 v/v)): δ 0.88 (t, 3H, $O(CH_2)_{17}$-CH_3), 1.27 (s, 30H, OCH_2CH_2-$(CH_2)_{15}$), 1.64 (s, 2H, OCH_2-CH_2), 1.90–2.28 (d, 2H, β-CH_2), 2.52 (s, 2H, γ-CH_2), 3.73 (s, 3H, OCH_3), 4.10 (s, 2H, OCH_2), 4.62 (s, 1H, α-CH).

2.8. Gel permeation chromatography (GPC)

GPC measurements of PtBuLGs and PtBuLG-*b*-PMLGSLGs were performed on a Waters ALC/GPC-150 with tetrahydrofuran (THF) as eluent, using polystyrene standards and the universal calibration method.

2.9. Thermogravimetric analysis (TGA)

TGA measurements were performed on a Perkin–Elmer thermogravimetric analyzer at a heating rate of 10 °C/min under nitrogen atmosphere. The block length ratio of $(tBuLG)_m$-*b*-$(MLGSLG)_n$ can be determined by:

$$\frac{n}{m} = \frac{185.2 \times (30.27 - WL)}{214.1 \times WL}$$

with *WL* (%) is the first step weight loss caused by the release of isobutylene, starting at 180 °C and ending at 250 °C.

2.10. Elemental analysis

The block length ratio of the diblock copolymer can be determined by:

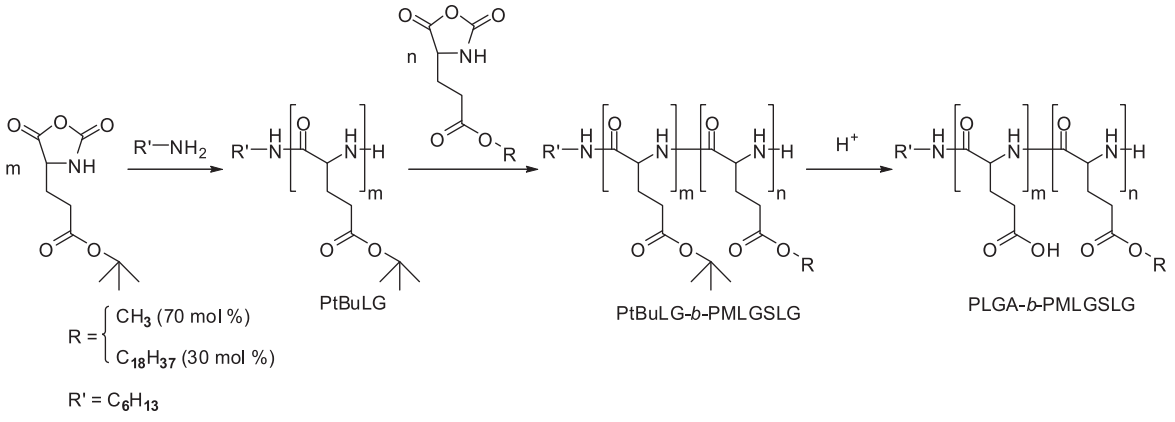

Scheme 1. Synthesis route of PLGA-*b*-PMLGSLG.

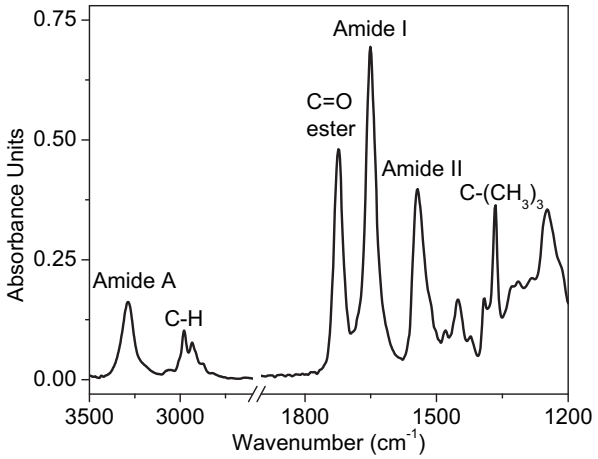

Fig. 1. ATR FT-IR spectrum of PtBuLG.

$$\frac{\%C}{\%N}(1) - \frac{\%C}{\%N}(2) = \frac{24m}{7(m+n)}$$

(1): of $(tBuLG)_m$-*b*-$(MLGSLG)_n$, (2): of corresponding $(LGA)_m$-*b*-$(MLGSLG)_n$ (after removing the *tert*-butyl protecting group using TFA).

2.11. Langmuir–Blodgett

π-A isotherms were measured using a home-modified computer-controlled Lauda Filmbalance (FW2), with an accuracy of 0.05 mN/m. The water used for the subphase was purified by reverse osmosis and subsequently through a Milli-Q filtration system. The pH of the subphase was adjusted by adding HCl (2N) or NaOH (1N) standard aqueous solutions (Aldrich). PLGA-*b*-PMLGSLGs were spread from *N*-methylpyrrolidone (NMP)/chloroform (3/7, v/v) solutions with 1–3% of acetic acid added, at concentrations of 0.4–0.6 mg/mL. PLGA was spread from a NMP/chloroform (3/7, v/v) solution at a concentration of 0.5 mg/mL. PMLGSLG was spread from a chloroform solution at a concentration of 0.5 mg/mL.

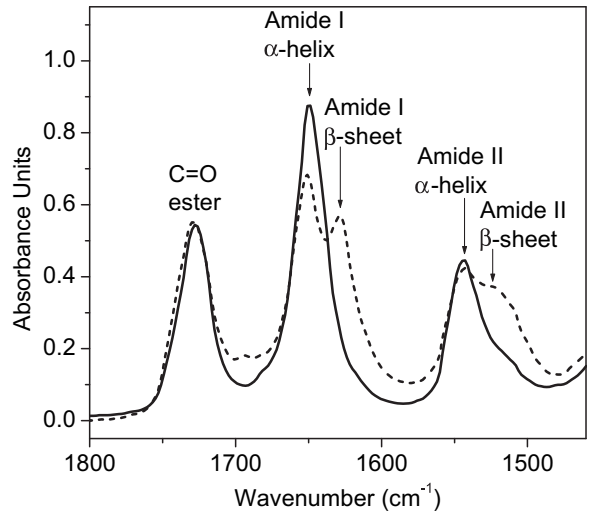

Fig. 2. ATR FT-IR spectra of PtBuLG-*b*-PMLGSLG synthesized under the optimal polymerization conditions (solid line) and PtBuLG-*b*-PMLGSLG synthesized under other normal conditions (short-dashed line).

(i) $I + M \xrightarrow{k_i} M_1^*$

(ii) $M_n^* + M \xrightarrow{k_p} M_{n+1}^*$, n = 1-7

(iii) $M_8^* + M \xrightarrow{k_p} M_9^*$

(iv) $v_i = k_i [M] [I]$

(v) $v_t = k_p [M_8^*] [M]$

Applying the steady state approximation:

(vi) $v_i = v_t$

(vii) $k_i [M] [I] = k_p [M_8^*] [M]$

(viii) $[M_8^*] = \frac{k_i}{k_p} [I]$

I = initiator, M = monomer, M_n^* = growing chain of DP n

Scheme 2. Simple steady state approximation in the reaction kinetics of NCA polymerization, assuming a steady state concentration of oligomers up to DP 9.

The double sided polished silicon wafers (Topsil Semiconductor Materials A/S, Frederikssund, Denmark, 1000 ± 25 μm thick) used as substrates were cleaned by treating them with a mixture of H_2O_2 (Merck, 30%)/NH_3 (Merck, 25%)/H_2O (1:1:5, v/v/v) for 30 min at 60 °C, followed by extensive rinsing with Milli-Q water, ultrasonication in a mixture of HCl (Merck, 37%)/H_2O (1:6, v/v) for 25 min, rinsing with Milli-Q water, and finally ultrasonication in methanol (Lab-Scan, 99.8%), methanol/chloroform (Lab-Scan, 99.5%), (1:1, v/v) and chloroform for 15 min. The cleaned silicon wafers were hydrophobized by treating them with a mixture of hexamethyldisilazane (Acros, 98%)/chloroform (1:4, v/v) at 50 °C, and rinsed with chloroform before use.

Deposition of LB films was carried out in the vertical mode. The subphase temperature was kept at 20 ± 0.1 °C. Transfer of a monolayer of $(LGA)_{63}$-*b*-$(MLGSLG)_{39}$ onto a hydrophilic substrate was done at 40 mN/m and at down- and upstroke speeds of 100 and 1 mm min^{-1}. Transfer of a monolayer of $(LGA)_{59}$-*b*-$(MLGSLG)_{82}$ onto a hydrophilic substrate was done at 35 mN/m and at down- and upstroke speeds of 100 and 10 mm min^{-1}. Monolayers were deposited onto both sides of the hydrophilic substrates during the

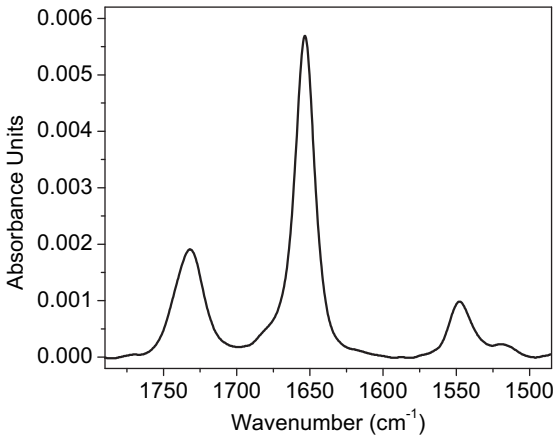

Fig. 3. Transmission FT-IR spectra of the cast film on a silicon wafer of PtBuLG-*b*-PMLGSLG in the completely α-helix structure.

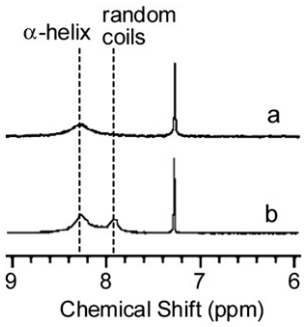

Fig. 4. ^{1}H NMR spectra for the range of 6–9 ppm of PtBuLG-*b*-PMLGSLG synthesized under the optimal polymerization conditions (a) and PtBuLG-*b*-PMLGSLG synthesized under other normal conditions (b).

upward stroke (Y-type). Transfer ratios were around unity (±10%). Additional layers were transferred on both down- and upstroke at the transfer speed of the first upstroke. A multilayer film (4 layers on each side of the substrate) of PMLGSLG was deposited onto a hydrophobized silicon substrate by Y-type transfer, at 20 mN/m and at down- and upstroke speeds of 3 mm min^{-1}.

2.12. Brewster angle microscopy (BAM)

A small Teflon trough (24.0 × 2.5 cm) was equipped with a quartz window flush in the middle bottom of the trough. Two hydrophobic barriers were moved symmetrically to change the surface area of the monolayer. BAM was performed using p-polarized light from a 10 mW argon laser beam set to an angle of 53.2° to the air–water interface. To magnify the reflected light from the monolayer a 50 mm planoconvex lens was used. An analyzer was used to enhance the contrast and a CCD camera was used for image recording.

2.13. Circular dichroism (CD) and linear dichroism (LD) spectroscopy

CD spectra of LB films on quartz plates were recorded on a Jasco J-815 spectropolarimeter. The quartz plate supporting the film was placed in the standard sample holder of the instrument. Different orientations of the quartz plate were analyzed to check for contributions from linear dichroism. The operating conditions were set as follows: bandwidth, 2 nm; scanning speed, 50 nm/min; D.I.T., 1 s; data pitch, 1 nm. Each spectrum was an accumulation of 5 scans.

LD measurements of LB films on quartz plates were performed using a Jasco J-815 spectropolarimeter. The operating conditions were set as follows: bandwidth, 2 nm; scanning speed, 200 nm/min; D.I.T., 1 s; data pitch, 1 nm.

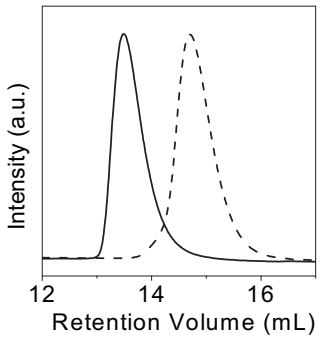

Fig. 5. GPC chromatograms (with THF as eluent) of $(tBuLG)_{59}$-*b*-$(MLGSLG)_{82}$ (solid line) and the corresponding PtBuLG macroinitiator (dashed line).

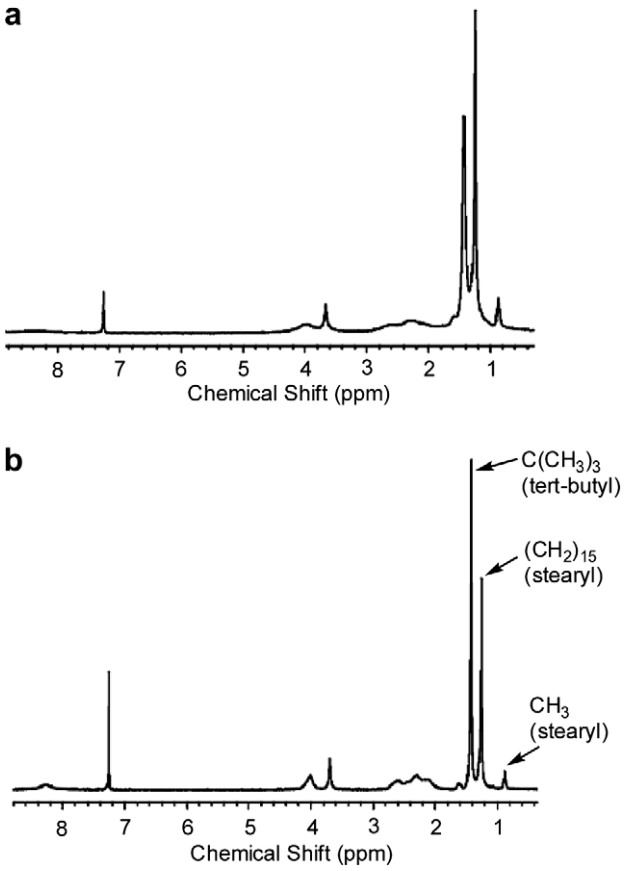

Fig. 6. ^{1}H NMR spectra of $(tBuLG)_{63}$-*b*-$(MLGSLG)_{39}$ in chloroform-d1 (a), and in chloroform-d1 with addition of a drop of TFA-d1 right before measuring (b).

2.14. IR measurements

Attenuated Total Reflection Fourier Transform Infrared (ATR FT-IR) measurements were carried out on a Bruker IFS88 FT-IR

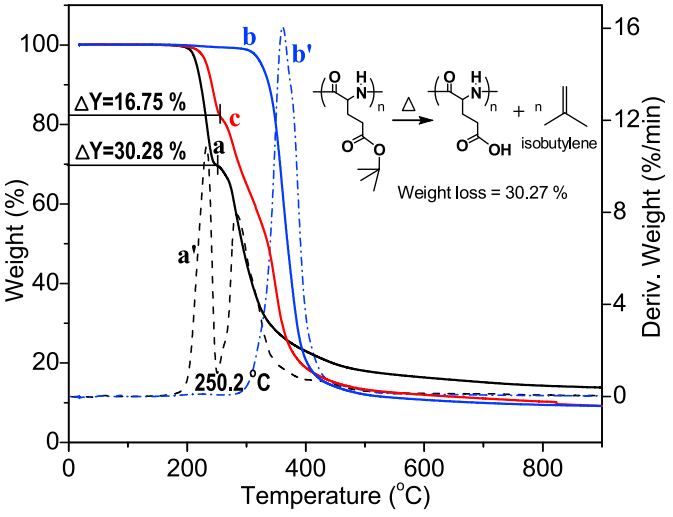

Fig. 7. TGA thermograms of PtBuLG (DP = 63) and its derivative (a and a′), PMLGSLG (DP = 118) and its derivative (b and b′), and $(tBuLG)_{63}$-*b*-$(MLGSLG)_{39}$ (c) recorded at a heating rate of 10 °C under nitrogen.

Table 1
Molecular weight properties of α-helical PtBuLG-*b*-PMLGSLGs prepared under the optimal polymerization conditions.

Entry	$(tBuLG)_m$			$(tBuLG)_m$-b-$(MLGSLG)_n$					
	m (^{1}H NMR)	m (GPC)	PDI (GPC)	Targeted *n*	n (^{1}H NMR)	n (TGA)	n (Elemen. Anal.)	n (GPC)	PDI (GPC)
1	63	66	1.34	40	39	44	41	52	1.24
2	59	58	1.16	85	82	83	80	88	1.15

spectrometer equipped with a MCT-A detector, at a resolution of 4 cm^{-1} and with an average of 50 scans.

Transmission Fourier Transform Infrared (FT-IR) measurements of cast films and LB films on double sided polished silicon substrates were performed at a resolution of 3 cm^{-1}, under vacuum on a Bruker IFS66 V/S FT-IR spectrometer equipped with a MIR DTGS detector. A sample shuttle accessory was used for interleaved sample and background scanning. A clean silicon substrate was used as the reference. Each spectrum is an average of 3 cycles of 120 scans for cast films and 40 cycles of 120 scans for LB films.

2.15. Small angle X-ray reflectivity

Small angle X-ray reflectivity measurements of LB films on silicon substrates were performed in θ/2θ geometry on a Philips X'pert materials research diffractometer (MRD) instrument, employing copper Kα radiation of 1.541 Å and with a divergence slit of 1/8°, an antiscatter slit of 1/4° and a progressive receiving slit of 0.3 nm. The X-ray tube was operated at V = 40 kV and I = 40 mA. For analysis, the measured reflectivity, R, was normalized by the Fresnel reflectivity, R_F. To model the electron density distribution along the *z*-direction, the film was divided into slabs (boxes) with thicknesses d_i, electron densities ρ_i and interface roughnesses σ_i between slabs i and i + 1, using a home-made computer program written in IDL 6.0 by Hibma [48]. A separate SiO_2 layer was not taken into account in the simulation, as this layer contributes insignificantly to the reflectivity of the wafer ($\rho_{SiO2}/\rho_{Si} = 0.95$) and could not be resolved from the reflectivity curves of bare silicon wafers [49].

3. Results and discussion

The PLGA-*b*-PMLGSLG amphiphilic diblock copolymer can be prepared via a diblock copolymer precursor, PtBuLG-*b*-PMLGSLG, which was synthesized employing the primary amine-initiated NCA polymerization via the synthesis route shown in Scheme 1.

3.1. Secondary structure of PtBuLG

A typical ATR FT-IR spectrum of PtBuLG is shown in Fig. 1. The polymer conformation is completely α-helical, as identified by the amide I absorption band at 1650 cm^{-1} and amide II absorption band at 1544 cm^{-1} [50]. Varying the reaction conditions (solvent, temperature and monomer concentration) in the synthesis of PtBuLGs with degrees of polymerization (DPs) in the range of 14–70 did not noticeably affect the polymer conformation.

3.2. Secondary structure of PtBuLG-b-PMLGSLG and the influence of polymerization conditions

Next, PtBuLG was used as macroinitiator to polymerize the PMLGSLG block. Because of the high propensity for β-sheet formation of the methyl-L-glutamate (MLG) residue [51–58], the PtBuLG-*b*-PMLGSLG diblock copolymers synthesized employing primary amine-initiated NCA polymerization under various conditions (solvent, temperature, concentration) were found to contain a considerable β-sheet content. The ATR FT-IR spectrum of one of these diblock copolymers is demonstrated by the short-dashed line in Fig. 2. The α-helix structure exhibits the FT-IR amide I and amide II bands respectively at 1652 and 1548 cm^{-1}, while the FT-IR amide I and amide II bands characteristic of the β-sheet structure are at 1626 and 1526 cm^{-1}. A small band caused by the antiparallel β-sheet amide I vibration is also observed at 1694 cm^{-1} [50].

For polypeptides to adopt the α-helix structure, a sufficiently long chain length is required. Below the critical chain length for helix stability (DP_c), oligopeptides take on the β-sheet form [59].

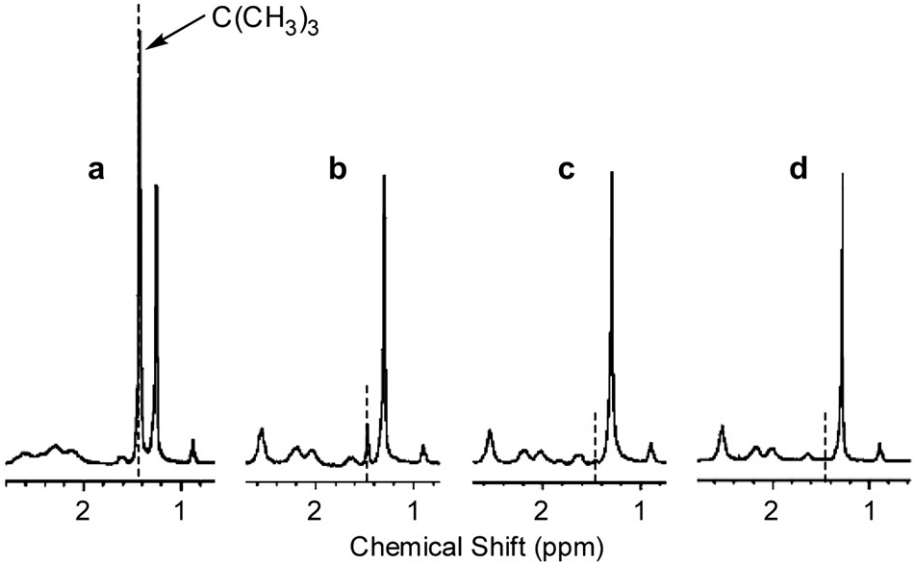

Fig. 8. ^{1}H NMR spectra of PtBuLG-*b*-PMLGSLG before hydrolysis (a) (chloroform-d1), and after hydrolysis in TFA for 15 min (b), 30 min (c), and 1 h (d) (chloroform-d1/TFA-d1 (2/1, v/v)).

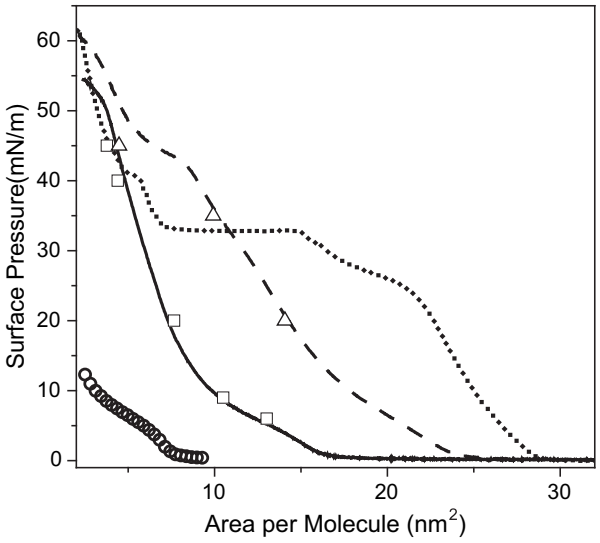

Fig. 9. π-A isotherms of $(LGA)_{63}$-*b*-$(MLGSLG)_{39}$ (solid line), $(LGA)_{59}$-*b*-$(MLGSLG)_{82}$ (dashed line), $(MLGSLG)_{118}$ (dotted line) and $(LGA)_{63}$ (open circles) on water surface at 20 °C. The compression speeds were ca. 38 $cm^2\,min^{-1}$ for $(MLGSLG)_{118}$ and ca. 19 $cm^2\,min^{-1}$ for the others. The open squares and triangles indicate stabilization points of $(LGA)_{63}$-*b*-$(MLGSLG)_{39}$ and $(LGA)_{59}$-*b*-$(MLGSLG)_{82}$, respectively.

The tendency to form β-sheets depends on the synthesis conditions and the association propensity of the amino acid residue [51,60]. A DP_c range has been reported for PMLG of 5–9 in dimethylformamide and m-cresol at 25 °C, whereas in dioxane these oligomers showed both α-helix and β-sheet structures [61,62]. The origin of the β-sheet formation from association through intermolecular hydrogen bonding of short peptide chains has been well established [52,59–67]. Kricheldorf et al. [68] concluded that the chain growth from β-sheet oligomer chains, in lamellar crystalline structure, is sterically inhibited. Thus, the associated oligomers precipitated during polymerization remain as a β-sheet fraction in the resulting polymer. Only oligopeptide chains which can be stabilized in the medium by either solvation or intramolecular hydrogen bonding continue to grow, reaching the length for helix stability [52,63]. The lengths of the β-sheet chains are mainly in a range of DP_c [62]. Hence, the formation of a stable α-helical structure is limited irrespective of the solvent used for film preparation.

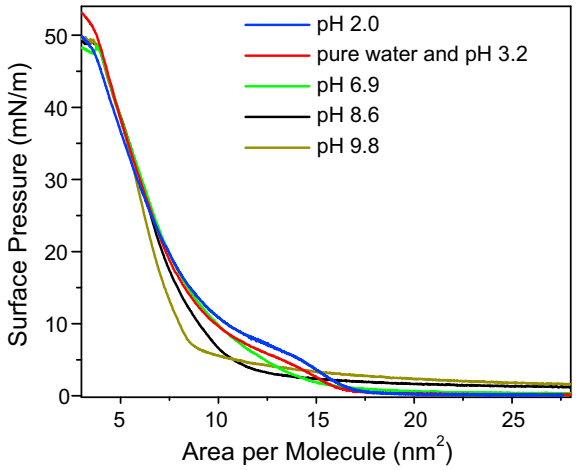

Fig. 10. π-A isotherms of $(LGA)_{63}$-*b*-$(MLGSLG)_{39}$ on water surface at 20 °C at various pH.

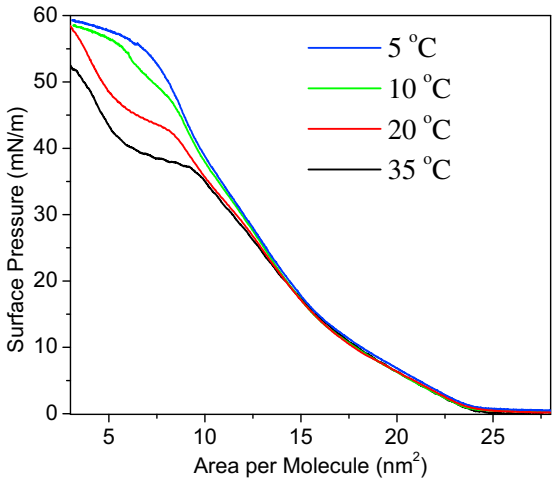

Fig. 11. π-A isotherms of $(LGA)_{59}$-*b*-$(MLGSLG)_{82}$ on water surface at different temperatures.

Since the β-sheet formation occurs in the oligomerization step, we found that to enhance the solubility of oligomers and to prevent them from intermolecular interactions via varying the reaction conditions (solvent, temperature, monomer concentration) increased the α-helix content of PtBuLG-*b*-PMLGSLG. Chloroform, compared with other more polar solvents such as dimethylformamide and tetrahydrofuran, was found to be the most helix-favorable solvent for PtBuLG-*b*-PMLGSLG. Such a nonpolar solvent solvates the long alkyl side chain and does not disrupt the intramolecular hydrogen bonds of the PMLGSLG block oligomers in the DP_c range, enhancing the stability of oligomers in the medium.

Lowering the temperature can generally decrease the polymer solubility; however, it also has a huge effect on the polymerization process. At a lower polymerization temperature of 0 °C, we observed a strong *decrease* in the oligomer aggregation. At an even lower temperature of −15 °C, the helicity content was increased even further but then the polymerization rate was too low. So, 0 °C was chosen as the optimal polymerization temperature for PtBuLG-*b*-PMLGSLG. The markedly increase in the α-helix content may be explained by the stabilization of the intramolecular hydrogen bonds of the oligomers, which are unstable and easily disrupted [62], in the DP_c range, DP 5 to 8, at a low temperature. Furthermore, a very low monomer concentration at 0.05 mol L^{-1} was found to give the optimal α-helix content. Although lowering the monomer

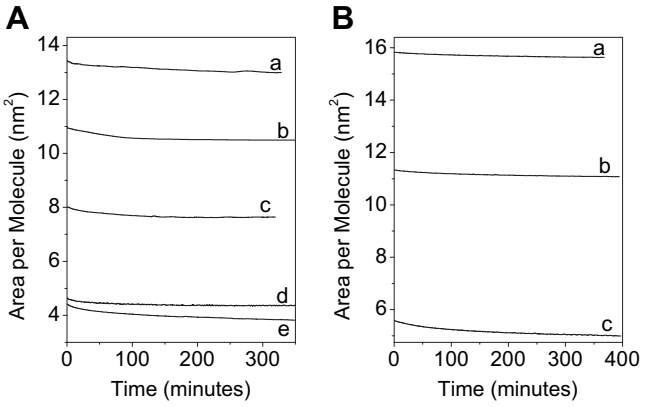

Fig. 12. A: stabilization curves of $(LGA)_{63}$-*b*-$(MLGSLG)_{39}$ at 6 (a), 9 (b), 20 (c), 40 (d) and 45 (e) mN/m; B: those of $(LGA)_{59}$-*b*-$(MLGSLG)_{82}$ at 20 (a), 35 (b), and 45 (c) mN/m.

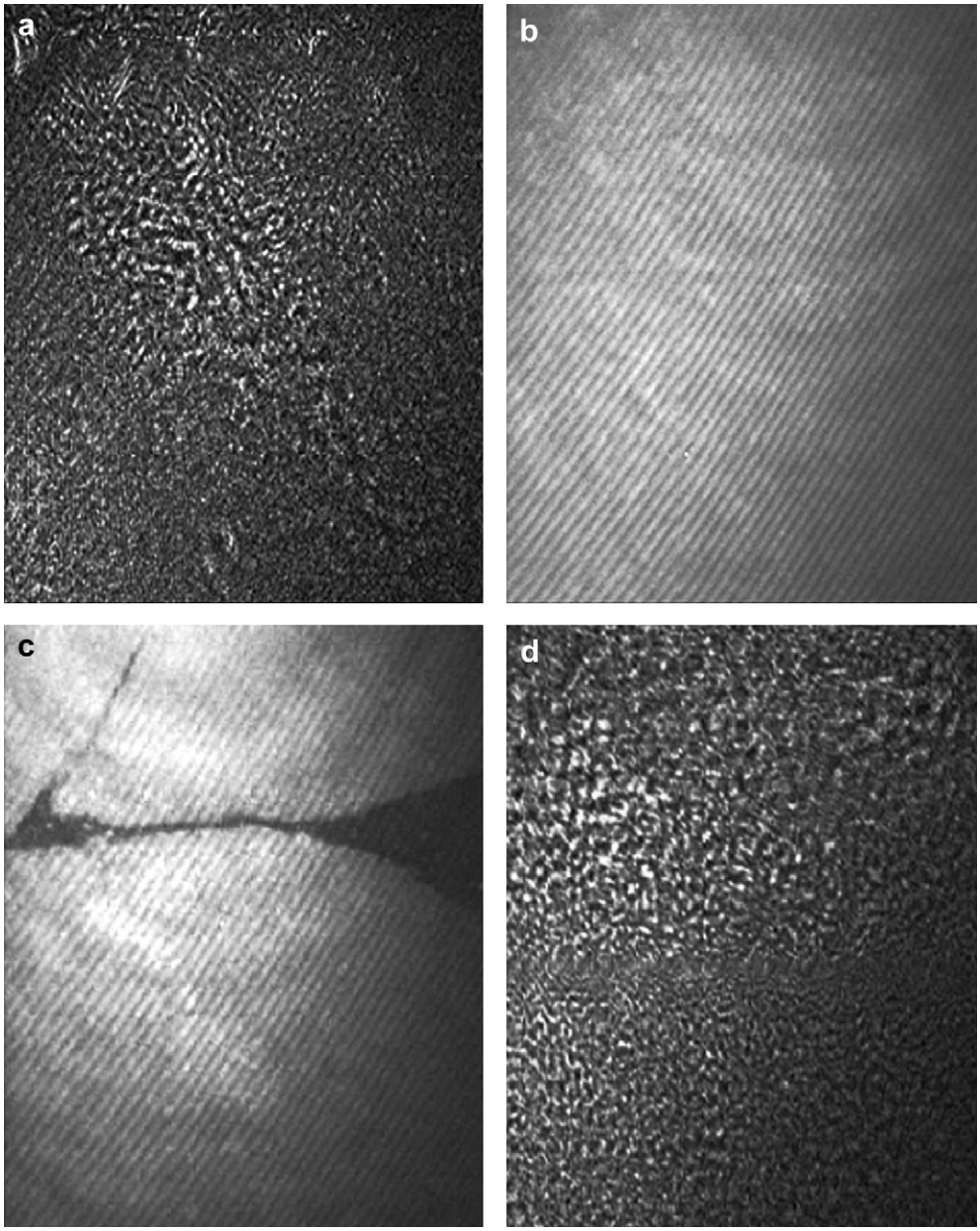

Fig. 13. BAM images (420 × 522 μm) of $(LGA)_{63}$-*b*-$(MLGSLG)_{39}$ during compression to 45 mN/m on a pure water surface at 20 °C, taken at $A = 32$ (a) and 17 (b) nm^2/molecule; those at $A = 17$ (c) and 32 (d) nm^2/molecule on subsequent decompression. The darkness in the images is the water; the regular inclined stripes are from the background.

concentration generally decreases the polymerization rate, the solubility of oligomers formed can be much enhanced in a dilute system and hence aggregation can be reduced during the oligomerization stage. Besides, by maintaining the monomer-to-initiator concentration ratio ([M]/[I]) constant, we in fact changed both monomer and initiator concentrations. The other, may be additional, effect can be seen from a simple steady state approximation of the reaction kinetics (Scheme 2). Assuming a steady state concentration of oligomers up to DP 9, we can derive a simple equation for the amount of oligomers (Equation viii, Scheme 2).

Using the optimal polymerization conditions as discussed above, PtBuLG-*b*-PMLGSLG was obtained with 100% α-helix content. As shown in the FT-IR spectra in Figs. 2 and 3, the complete α-helix structure of PtBuLG-*b*-PMLGSLG is identified by the characteristic α-helix amide I and amide II bands at 1649 cm^{-1} and 1545 cm^{-1}, respectively, and by the absence of the amide bands corresponding to the β-sheet structure. Also, the diblock copolymer secondary structure was confirmed by ^1H NMR in $CDCl_3$ containing 10% of TFA-d1 (Fig. 4). In the presence of TFA, the β-sheet oligopeptides are transformed into random coils and can be dissolved [57]. The chemical shift of the amide N–H signal was detected at 8.27 ppm for the α-helix. The ^1H NMR spectra of α-helical polyglutamates (such as PtBuLG and PMLGSLG polymerized with triethylamine) in $CDCl_3$ without adding TFA-d1 showed the same N–H chemical shift, indicating that the α-helix structure is preserved in the $CDCl_3$/TFA-d1 solvent mixture. An upfield shift to 7.89 ppm was observed for the random coils. As shown in Fig. 4, the ^1H NMR result is in good agreement with the ATR FT-IR and transmission FT-IR findings.

3.3. Molecular weight characterization of PtBuLG-*b*-PMLGSLG

The molecular weight properties of the PtBuLG macroinitiator and PtBuLG-*b*-PMLGSLG were first characterized by GPC employing

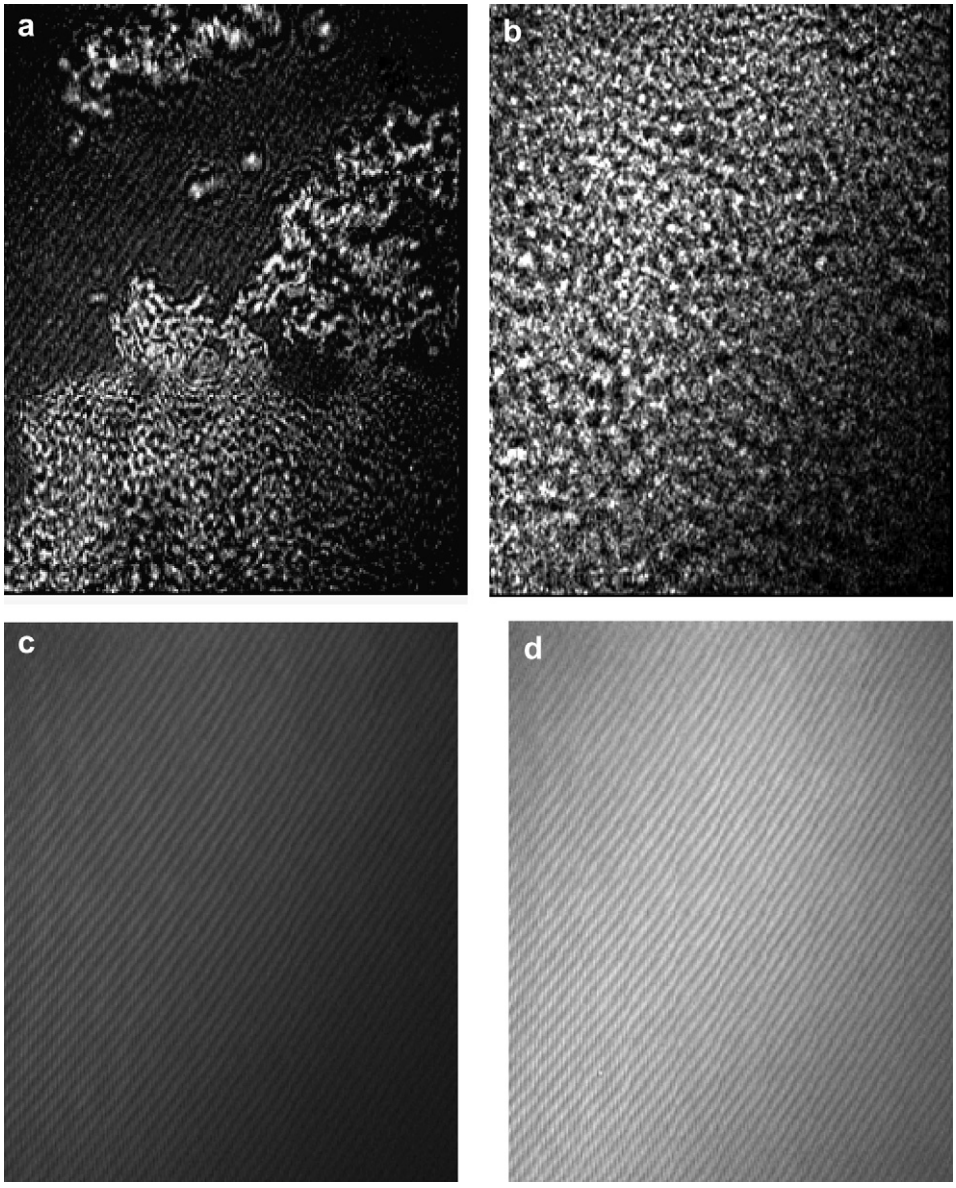

Fig. 14. BAM images (420 × 522 μm) of $(LGA)_{63}$-*b*-$(MLGSLG)_{39}$ during compression to 45 mN/m, at 20 °C and a subphase pH of 2, taken at $A = 32$ (a) and 25 (b) nm^2/molecule; those at a subphase pH of 8.6 taken at $A = 30$ (c) and 12 (d) nm^2/molecule. The darkness in the images is the water; the regular inclined stripes are from the background.

the method of universal calibration, with tetrahydrofuran (THF) as eluent and polystyrene standards. The reliability of the measurements is supported by the findings of Temyanko et al. [69] showing the validity of universal calibration for stiff α-helical polypeptides over a range of molecular weights in appropriate solvents. More particularly, the universal calibration plot for PSLG with M_w in a range of 13 000–250 000 in THF overlays with that for polystyrene [69]. In our experiments, THF was found to be a good solvent for the α-helical conformers of PtBuLG and PtBuLG-*b*-PMLGSLG. Their solubility is favored by the bulky *tert*-butyl group and extended stearyl side chains surrounding the backbone rods [70]. THF has also been used for GPC analysis of PMLGSLG [9].

Besides the diblock copolymer compositional confirmation by ^{1}H NMR, the shift to a higher molecular weight in the GPC chromatogram of PtBuLG-*b*-PMLGSLG, compared with the PtBuLG macroinitiator, proves the formation of the diblock copolymer (Fig. 5). The absence of a trace of a molecular weight fraction corresponding to PtBuLG in the chromatogram of PtBuLG-*b*-PMLGSLG clearly indicates the absence of homopolymer impurity.

^{1}H NMR was used as an alternative method to characterize the molecular weights of PtBuLG and PtBuLG-*b*-PMLGSLG. The DP of PtBuLG was estimated using the integral ratio of the signal of the *tert*-butyl group ($(CH_3)_3$, 1.42 ppm) and that of the methyl group (CH_3, 0.87 ppm) of the *n*-hexylamine initiator incorporated in the polymer chain. The block length ratio of PtBuLG-*b*-PMLGSLG was determined by comparing the peak integral of the *tert*-butyl group (9H, 1.42 ppm) with that of the stearyl group (30H, 1.25 ppm). Because of hydrogen bonding, the ^{1}H NMR peaks were not clearly separated (Fig. 6a). High-temperature ^{1}H NMR measurements (in 1,2-dichlorobenzene-d4 or NMP-d9 at 130 °C) of PtBuLG-*b*-PMLGSLG did not give spectra with much improved peak separation. Instead, 1–2 small drops of TFA-d1 was added to the diblock copolymer solution in chloroform-d1 immediately before measuring, resulting in good peak separation (Fig. 6b). It should be noted that the presence of TFA might result in partial removal of the *tert*-butyl group. However, the amount of TFA was relatively small and the samples were measured in a short time, thus loss of the *tert*-butyl group should be negligible.

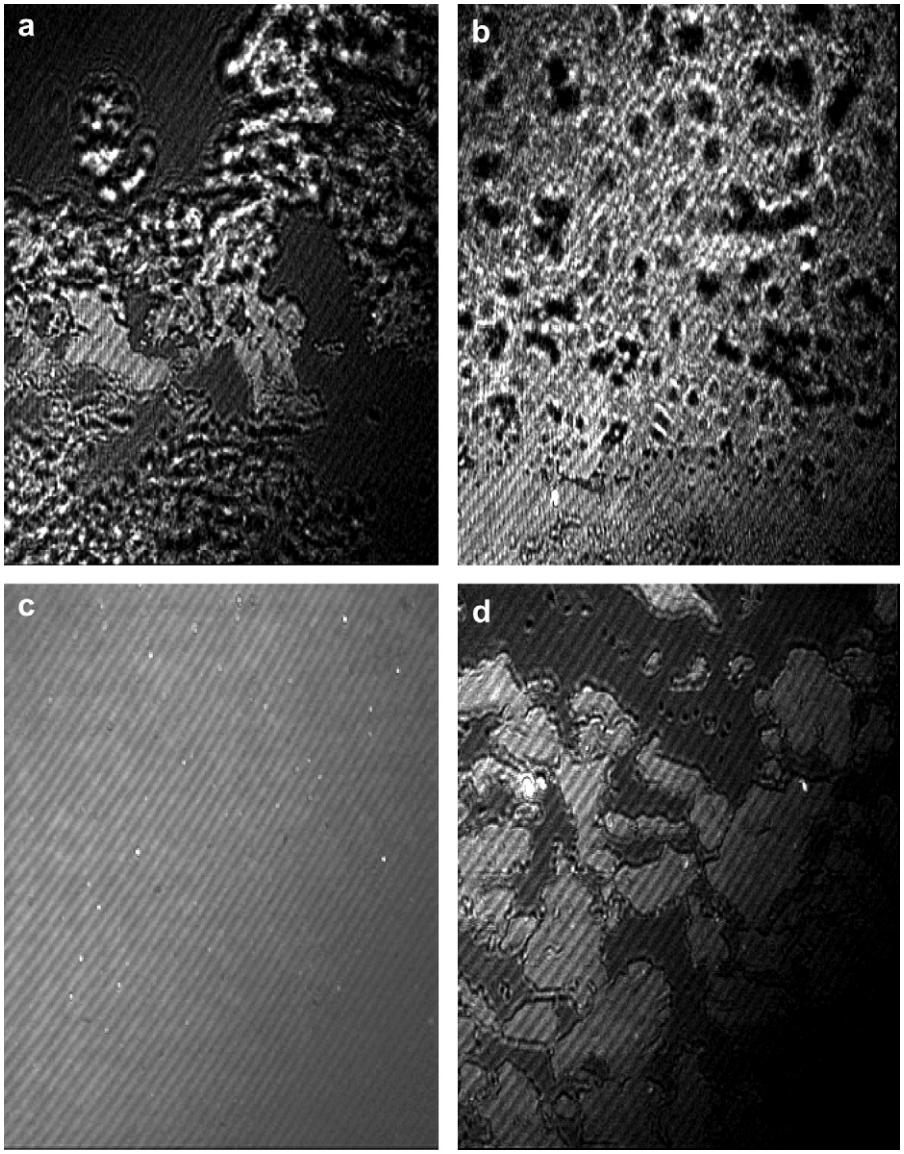

Fig. 15. BAM images (420 × 522 μm) of $(LGA)_{59}$-*b*-$(MLGSLG)_{82}$ on a pure water surface during compression to 50 mN/m, taken at $A = 39$ (a), 27 (b) and 23 (c) nm^2/molecule; that at $A = 29$ nm^2/molecule on subsequent decompression (d). The darkness in the images is the water; the regular inclined stripes are from the background.

In addition, TGA and elemental analysis were used as supporting methods to confirm the results of GPC and ^1H NMR in the determination of the block length ratio. In the TGA method, the *tert*-butyl ester group is thermolyzed to yield the carboxylic acid and release isobutylene gas, starting at 180 °C and ending at 250 °C (Fig. 7). The weight loss of 30.28% is in good agreement with the theoretical value (30.27%) for *tert*-butyl group elimination. The ATR-FTIR spectrum of PtBuLG-*b*-PMLGSLG after heating to 250 °C

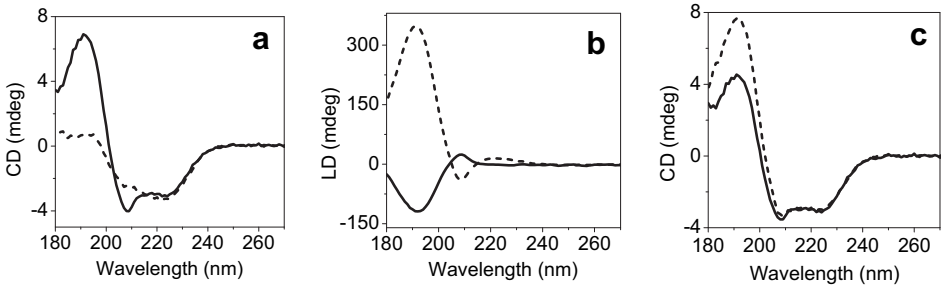

Fig. 16. Apparent CD spectra (a), LD spectra (b) and corrected CD spectra (c) of the multilayer LB film (3 layers on each side of the quartz substrate) of $(LGA)_{63}$-*b*-$(MLGSLG)_{39}$ deposited at 40 mN/m. The sample was analyzed in two different directions: horizontal orientation (solid line) and vertical orientation (dashed line). The corrected CD spectra are the corresponding apparent CD spectra (CD_{app}) corrected for LD contributions according to $CD = CD_{app} + 0.02\ LD$ [74].

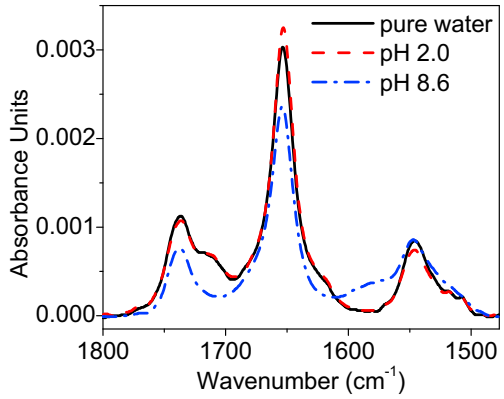

Fig. 17. Transmission FT-IR spectra of the LB monolayers (on both sides of the silicon substrate) of $(LGA)_{63}$-*b*-$(MLGSLG)_{39}$ deposited at 40 mN/m. Prior to LB deposition, the diblock copolymer was spread either on pure water or at different subphase pH.

did not show any peaks indicating the formation of either an anhydride or imide group. This indicates that no pyrolysis of the resulting carboxylic group accompanies the first weight loss step caused by removal of the *tert*-butyl group. Since PMLGSLG is stable up to 250 °C, the block length ratio of PtBuLG-*b*-PMLGSLG can be derived from the measured weight loss of this step. In the elemental analysis method, the block length ratio was derived from the change in the elemental contents upon removal of the *tert*-group by hydrolysis.

As shown in Table 1, the results obtained from the different methods are in good agreement. Polymerization of the PMLGSLG block initiated by PtBuLG yielded diblock copolymers with DPs close to the targeted values and small polydispersities. In addition to preventing early precipitation by complete suppression of β-sheet formation, performing the polymerization at a low temperature seems to prevent side reactions [71].

3.4. Removal of the tert-butyl group

Complete removal of the *tert*-butyl group was confirmed by disappearance of the ^{1}H NMR *tert*-butyl peak at 1.42 ppm in chloroform-d1/TFA-d1 (2/1, v/v) (Fig. 8). In addition, the ATR-FTIR spectrum of the copolypeptide after hydrolysis showed the disappearance of the signals of the *tert*-butyl deformation and stretching

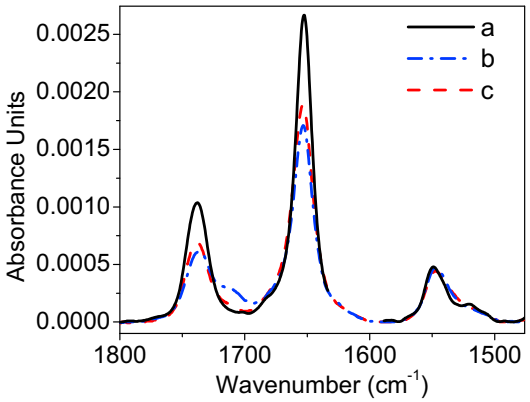

Fig. 18. Transmission FT-IR spectra of the LB films on double sided polished silicon substrates of $(MLGSLG)_{118}$ (96% of α-helix structure, 4 layers on each side of the substrate, transferred at 20 mN/m) (a), $(LGA)_{63}$-*b*-$(MLGSLG)_{39}$ (monolayer on each side of the substrate, transferred at 40 mN/m) (b), and $(LGA)_{59}$-*b*-$(MLGSLG)_{82}$ (monolayer on each side of the substrate, transferred at 35 mN/m) (c). For comparison, the spectral absorption intensities are normalized relative to the height of the amide II band.

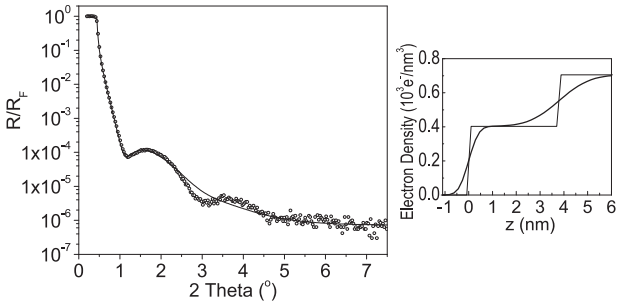

Fig. 19. Left-hand side: best one-slab fit to the X-ray reflectivity curve of the monolayer LB film of $(LGA)_{63}$-*b*-$(MLGSLG)_{39}$ transferred onto a silicon substrate at 40 mN/m; the dots represent the experimental data and the full line represents the fitted curve. Right-hand side: electron density profile corresponding to the curve fit (smooth curve); for clarity the same electron density profile is shown assuming all interface roughnesses to be zero (step-like curve).

vibrations at 1367 cm^{-1} and 2977 cm^{-1}. A carboxylic absorption band appeared at 1711 cm^{-1}, along with a decrease in intensity of the carbonyl absorption band at 1728 cm^{-1}. A broad band characteristic of the bonded O–H stretching vibration also appeared between 3400 and 2500 cm^{-1}. The stability of the amide main chain and the ester side chains of the PMLGSLG block upon the *tert*-butyl ester hydrolysis process was ascertained by treating PMLGSLG with TFA under the same hydrolysis conditions. The ATR FT-IR and GPC results of PMLGSLG, before and after acid treatment, indicated that the molecular weight of the diblock copolymers was preserved after removal of the *tert*-butyl group.

After having successfully prepared the α-helical PLGA-*b*-PMLGSLG amphiphilic diblock copolymers, we subsequently studied their monolayer behavior.

3.5. Surface pressure-area (π-A) isotherm

Fig. 9 shows the π-A isotherms for $(LGA)_{63}$-*b*-$(MLGSLG)_{39}$ and $(LGA)_{59}$-*b*-$(MLGSLG)_{82}$ spread on a pure water surface at 20 °C, in comparison with those for PLGA (DP = 63) and PMLGSLG (DP = 118). The isotherm of PLGA, spread on pure water, was similar to that reported for sodium salt of PLGA (DP = 405) at a water subphase pH

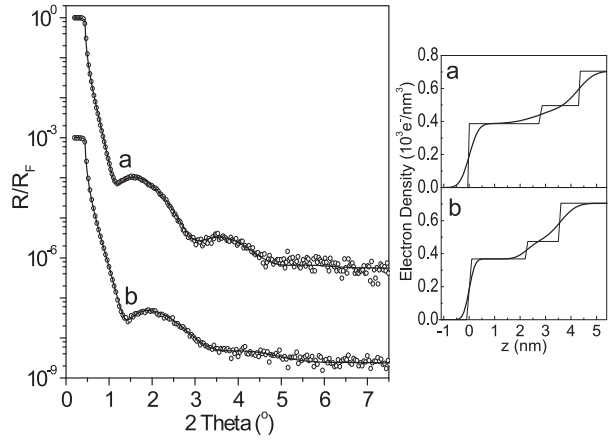

Fig. 20. Left-hand side: two-slab fits to the X-ray reflectivity curves of the monolayer LB film of $(LGA)_{63}$-*b*-$(MLSGLS)_{39}$ transferred onto a silicon substrate at 40 mN/m (a) and the monolayer LB film of $(LGA)_{59}$-*b*-$(MLSGLS)_{82}$ transferred onto a silicon substrate at 35 mN/m (b); the dots represent the experimental data and the full lines represent the fitted curves; curve b is shifted vertically for clarity. Right-hand side: electron density profiles corresponding to the curve fits (smooth curves); for clarity the same electron density profiles are shown assuming all interface roughnesses to be zero (step-like curves).

Table 2
Two-slab fit parameters for the curve fits shown in Fig. 20.

	$(LGA)_{63}$-*b*-$(MLGSLG)_{39}$ $\pi = 40$ mN/m	$(LGA)_{59}$-*b*-$(MLGSLG)_{82}$ $\pi = 35$ mN/m
Layer thickness (nm)		
L_1 (PLGA)	1.51	1.30
L_2 (PMLGSLG)	2.80	2.26
Total thickness	4.31	3.56
Electron density ρ_i (10^3 e^-/nm^3)		
ρ_0 (silicon)	0.705[a]	0.705[a]
ρ_1 (PLGA)	0.496	0.474
ρ_2 (PMLGSLG)	0.387	0.368
Interface roughness (nm)		
σ_{01} (silicon/PLGA)	0.48 ± 0.04[a, b]	0.48 ± 0.04[a, b]
σ_{12} (PLGA/PMLGSLG)	0.82	0.35
σ_{23} (PMLGSLG/air)	0.29	0.18

[a] Values kept fixed for the curve fits.
[b] The average roughness of bare silicon wafers.

of 3 [72]. PLGA is surface active to some extent, exhibiting a transition at a low surface pressure of ca. 5–7 mN/m. The isotherm of PMLGSLG has been reported in literature [9], showing a steep rise in pressure upon compression due to the packing of the α-helices lying flat on the water surface, followed by a liquid-condensed phase. Upon further compression, the monolayer of PMLGSLG collapses, indicated by a plateau transition at about 33 mN/m. The isotherms of the PLGA-*b*-PMLGSLG diblock copolymers displayed a completely different behavior. Upon compression, first a transition analogous to the isotherm of PLGA spread under the same condition is detected, and then there is a linear increment in surface pressure. For $(LGA)_{59}$-*b*-$(MLGSLG)_{82}$ with the longer hydrophobic block, another transition above 40 mN/m appears.

The first transition at 5–10 mN/m can be assigned to the water immersion of the PLGA block. Hence, varying the subphase pH can influence the transition. Fig. 10 demonstrates the effect of subphase pH on this transition. At high pH, upon spreading the helix-to-coil conformational change of the PLGA block results in surface area constraints caused by coil expansion, indicated by a low surface pressure recorded even at a very large area. Upon compression, a large decrease in surface area with a very small increase in surface pressure implies a facile water-solubilization of the PLGA block at high pH. At pH 3.2, the isotherm is identical to that measured on pure water. At low pH, up to 2.0, the first transition is shifted to a slightly higher pressure due to the diminished solubility of the PLGA block.

The second transition above 40 mN/m, only observed for $(LGA)_{59}$-*b*-$(MLGSLG)_{82}$, was affected by changing temperature. As shown in Fig. 11, increasing the temperature from 5 to 35 °C shifts the transition to lower surface pressures and the isotherm beyond that to smaller surface areas. This suggests that the transition reflects reorganization, favored at elevated temperatures, of the PMLGSLG segments.

The high collapse surface pressures, at 50–55 mN/m, and high compressibilities of the PLGA-*b*-PMLGSLG monolayers compared with PMLGSLG suggest that the diblock copolymer molecules are oriented out of the water surface to form a double-brush. The molecular surface areas of PLGA-*b*-PMLGSLGs at high surface pressures, of 35–45 mN/m, where the monolayers are still stable and transferable, lies in the range of the helix cross-sectional area of PMLGSLG, of 2.4–9.6 nm^2 [9,13], depending on the molecular packing and the side chain configuration. This suggests that upon high compression, the helices are oriented with a tilt away from the water surface.

3.6. Stabilization

Fig. 12 displays the stabilization curves of $(LGA)_{63}$-*b*-$(MLGSLG)_{39}$ and $(LGA)_{59}$-*b*-$(MLGSLG)_{82}$ performed at different surface pressures. Stable, transferable monolayers were obtained with transfer ratios of around unity over a range of surface pressures. Indicated by stabilization points in Fig. 9, the molecular areas at which the monolayers stabilize are in good agreement with the π-A isotherms, indicating the absence of relaxation effects. Only above the second transition in the isotherm recorded for $(LGA)_{59}$-*b*-$(MLGSLG)_{82}$, e.g. at 45 mN/m, does the stabilization point shift to a smaller area. This implies that this transition, which might be related to rearrangement of the chains, is a rather slow process. Though the monolayer is stabilized at 45 mN/m, film deposition resulted in an incomplete transfer, probably because at this state the monolayer does not maintain its molecular mobility.

3.7. Surface imaging by BAM

BAM images taken during the compression-decompression process on a pure water surface and at different subphase pH are shown for PLGA-*b*-PMLGSLGs in Figs. 13–15. On spreading on a pure water surface, there exist monolayer islands with gaps of water surface in between. Compression reduces the water gaps and as soon as the surface pressure is built up, a homogeneous monolayer is formed. For both PLGA-*b*-PMLGSLGs, no monolayer collapse was detected upon compression to 45–50 mN/m. Upon decompression the monolayer first ruptures and then reverts back to the initial state. It has been reported for PBLG that the molecules self-aggregate without external pressure into 2D islands of single molecule thickness on the water surface [73]. Compared with PBLG, on a pure water surface, $(LGA)_{63}$-*b*-$(MLGSLG)_{39}$ forms much smaller aggregates (Fig. 13). This is most likely due to the interaction between the long PLGA hydrophilic block and the water subphase, limiting mutual antiparallel attractions between molecules. In agreement with this explanation, when increasing the surface activity of the diblock copolymers by either decreasing the subphase pH or increasing $DP_{PMLGSLG}$, more monolayer self-aggregate formation is found to occur, as shown in Fig. 14a, b and 15. On the contrary, at a high pH of 8.6, where the PLGA block is fully charged, no aggregate was observed (Fig. 14c and d). The water-solubilization of the PLGA block at this pH leads to molecular reorientation in a manner favoring a double-brush formation, preventing antiparallel orientations of the helices.

3.8. CD spectra of LB films

LB films of the PLGA-*b*-PMLGSLG diblock copolymers were transferred onto both sides of hydrophilic substrates. Homogeneous and uniform films were obtained, as demonstrated by atomic force microscopy (tapping mode). Fig. 16 shows typical CD spectra corrected for linear dichroism (LD) contributions [74], analyzed in different directions in the spectropolarimeter, of a multilayer LB film of PLGA-*b*-PMLGSLG. The LD effect was caused by preferential orientation of the α-helices along the dipping direction [9]. The corrected spectra analyzed in different directions are in agreement with each other, showing one maximum at 191 nm and two minima at 208 and 222 nm. These are the characteristic bands for the right-handed α-helical polypeptides [51,74].

3.9. Transmission FT-IR spectra of LB films

Fig. 17 shows representative transmission FT-IR spectra of the LB monolayers of PLGA-*b*-PMLGSLG prepared on pure water and at different subphase pH. At subphase pH 8.6, the C=O stretching band of the hydrogen bonded carboxyl group at 1711 cm^{-1} disappears and the ionized carboxyl band appears at 1560 cm^{-1}, indicating the helix-to-coil conformational change of the PLGA block. The spectra of the monolayers prepared on pure water and at

subphase pH 2 are identical to each other, showing the characteristic α-helix amide I and amide II bands at 1653 and 1548 cm^{-1}. This indicates that even when PLGA-*b*-PMLGSLG was spread on a pure water surface, the α-helix structure was predominant. PLGA has been reported to form a completely α-helix structure in aqueous solution of pH below 5. Its transition between the α-helical and random coil conformations occurs in the region of pH 5 to 6, where the α-helix percentage decreases to 80–70% [51]. The predominant α-helix structure of the PLGA-*b*-PMLGSLG monolayer on a pure water surface is in part due to the surface water being rather acidic (pH about 5.5), arising from a large amount of atmospheric CO_2 dissociating in the subphase. Besides, the degree of charging of the PLGA block depends on the local pH inside the PLGA brush, which can be slightly lower than the pH in the subphase at a high brush density [75]. Studies of the helix–coil transition of PLGA in aqueous solutions containing osmolytes have shown that increasing the osmotic pressure favors more α-helix structure over hydrated coils [76,77]. Hence, the osmotic pressure inside the PLGA brush may enhance the stability of the α-helix structure. As a result, for a PLGA brush, the helix–coil transition pH could be raised to a higher value than observed for PLGA in solution. In fact, a pH range for the helix–coil transition of a surface-grafted PLGA film has been reported to be 5.75–7 [78].

Fig. 18 compares the transmission FT-IR spectra of the LB monolayer films of $(LGA)_{63}$-*b*-$(MLGSLG)_{39}$ and $(LGA)_{59}$-*b*-$(MLGSLG)_{82}$, transferred onto silicon substrates at 40 and 35 mN/m, respectively, with that of an LB multilayer film of PMLGSLG. From the absorption intensity ratio of the amide I and amide II bands the average helix tilt angle in the monolayers can be determined [13]. A higher amide I/amide II band area ratio (AI/AII) corresponds to a larger tilt angle between the helices and the surface normal [13]. Since the PMLGSLG helices in an LB film are oriented parallel to the substrate surface [9], the helix tilt angle is 90° and AI/AII has its maximum value for this system. As seen in Fig. 18, for the PLGA-*b*-PMLGSLG monolayers, the AI/AII ratios are much lower than that for the PMLGSLG LB film, suggesting average helix tilt angles much smaller than 90°. This is a clear indication of double-brush monolayer formation, in which the diblock copolymer helices are tilted away from the substrate surface.

3.10. Small angle X-ray reflectivity

Curve fits to the X-ray diffractograms measured for the PLGA-*b*-PMLGSLG monolayer LB films were at first performed with one-slab models. The best one-slab fit to the reflectivity curve of the monolayer LB film of $(LGA)_{63}$-*b*-$(MLGSLG)_{39}$ is shown in Fig. 19. However, the curve fit is insufficient at high scattering angles. Instead, as shown in Fig. 20, the two-slab models result in good fits of the reflectivity curves for the monolayer films of PLGA-*b*-PMLGSLGs. The first slab is assumed for the PLGA layer and the second slab for the PMLGSLG layer. Table 2 shows the two-slab fit parameters for the PLGA-*b*-PMLGSLG monolayer films. From the density values reported for PLGA and PMLGSLG [31,32,51,79], the electron densities of PLGA and PMLGSLG lie in the ranges of 0.473×10^3–0.503×10^3 e^-/nm^3 and 0.360×10^3–0.381×10^3 e^-/nm^3, respectively. Thus, the determined values in the two-slab fits shown in Table 2 are reasonable. The good fits using the two-slab models give ample evidence for the double-brush structure of the monolayer films.

Taken together, the above results clearly demonstrate that the PLGA-*b*-PMLGSLG diblock copolymers form stable monolayers with the α-helical chains tilted to the surface normal. Moreover, the resulting monolayers are well-transferred onto solid substrates with the double-brush structure retained. However, factors such as the chain lengths, which might influence the molecular orientation and the double-brush structure, as well as other effects such as the introduction of anisotropy during the transfer process still need to be investigated in order to fully understand and control the film properties.

4. Conclusions

We have found that the polymerization conditions strongly affect the α-helix to β-sheet content ratio of the PtBuLG-*b*-PMLGSLG diblock copolymer. Taking into account the effects of several factors including solvent, temperature and monomer concentration on oligomer stabilization, the reaction conditions can be tuned to significantly enhance the α-helix content. The diblock copolymers were obtained in a completely α-helical structure, with close-to-designed DPs and small polydispersities.

After removal of the *tert*-butyl group, the resulting amphiphilic PLGA-*b*-PMLGSLG diblock copolymers formed a stable α-helical double-brush structure in monolayers at the air–water interface and in LB films, as evidenced by the π-A isotherm, transmission FT-IR and X-ray reflectivity results. The 3–5 nm thick monolayer films obtained with unidirectionally aligned helix macrodipoles can provide an extremely large electric field across the peptide monolayers. Such directional properties and the liquid-like matrix provided by the amorphous stearyl side chain make these films suitable for functionalization with various bio- and optical molecules with potential applications as functional materials.

Acknowledgments

We thank Gert Alberda van Ekenstein for his help with TGA measurements. This research is supported by NanoNed, a nanotechnology program of the Dutch Ministry of Economic Affairs.

References

[1] Kawaguchi T, Nakahara H, Fukuda K. Thin Solid Films 1985;133:29–38.
[2] Winter CS, Tredgold RH, Vickers AJ, Khoshdel E, Hodge P. Thin Solid Films 1985;134:49–55.
[3] Bubeck C, Neher D, Kaltbeitzel A, Duda G, Arndt T, Sauer T, et al. NATO ASI Ser E Appl Sci 1989;162:185–93.
[4] Bubeck C, Arndt T, Sauer T, Duda G, Wegner G. RSC Spec Publ 1989;69:344–7.
[5] Wegner G. Macromol Chem Phys 2003;204:347–57.
[6] Sekkat Z, Knoll W. Adv Photochem 1997;22:117–95.
[7] Wegner G. Mol Cryst Liq Cryst 1992;216:7–12.
[8] Tredgold RH. J Chem Phys 1988;85:1079–80.
[9] Duda G, Schouten AJ, Arndt T, Lieser G, Schmidt GF, Bubeck C, et al. Thin Solid Films 1988;159:221–30.
[10] Schwiegk S, Vahlenkamp T, Xu Y, Wegner G. Macromolecules 1992;25:2513–25.
[11] Whitesell JK, Chang HK. Science 1993;261:73–6.
[12] Oosterling MLCM, Willems E, Schouten AJ. Polymer 1995;36:4463–70.
[13] Wieringa RH, Siesling EA, Werkman PJ, Angerman HJ, Vorenkamp EJ, Schouten AJ. Langmuir 2001;17:6485–90.
[14] Luijten J, Groeneveld DY, Nijboer GW, Vorenkamp EJ, Schouten AJ. Langmuir 2007;23:8163–9.
[15] Jaworek T, Neher D, Wegner G, Wieringa RH, Schouten AJ. Science 1998;279:57–60.
[16] Morita T, Kimura S, Kobayashi S, Imanishi Y. J Am Chem Soc 2000;122:2850–9.
[17] Yokoi H, Hayashi S, Kinoshita T. Prog Polym Sci 2003;28:341–57.
[18] Toyotama A, Kugimiya S, Yonese M, Kinoshita T, Tsujita Y. Chem Lett 1997;26:443–4.
[19] Hosokawa H, Kinoshita T, Tsujita Y, Yoshimizu H. Chem Lett 1997;26:745–6.
[20] Kishihara K, Kinoshita T, Mori T, Okahata Y. Chem Lett 1998;27:951–2.
[21] Doi T, Kinoshita T, Tsujita Y, Yoshimizu H. Bull Chem Soc Jpn 2001;74:421–5.
[22] Yokoi H, Kinoshita T. Chem Lett 2004;33:426–7.
[23] Niwa M, Takada T, Higashi N. J Mater Chem 1998;8:633–6.
[24] Higashi N, Koga T, Niwa M. Langmuir 2000;16:3482–6.
[25] Watanabe J, Sakajiri K, Okoshi K, Kawauchi S, Magoshi J. Macromol Chem Phys 2001;202:1004–9.
[26] Watanabe J, Fukuda Y, Gehani R, Uematsu I. Macromolecules 1984;17:1004–9.
[27] Wegner G. Thin Solid Films 1992;216:105–16.
[28] Kurthen C, Nitsch W, Stöckelhuber W. Makromol Chem Macromol Symp 1991;46:371–5.
[29] Schwiegk S, Vahlenkamp T, Wegner G, Xu Y. Thin Solid Films 1992;210-211:6–8.

[30] Wegner G. Mol Cryst Liq Cryst 1993;235:1–34.
[31] Schmidt A, Mathauer K, Reiter G, Foster MD, Stamm M, Wegner G, et al. Langmuir 1994;10:3820–6.
[32] Vierheller TR, Foster MD, Schmidt A, Mathauer K, Knoll W, Wegner G, et al. Macromolecules 1994;27:6893–902.
[33] Shibata A, Bekku Y, Ueno S, Yamashita S. Langmuir 1994;10:3723–6.
[34] Mathauer K, Schmidt A, Knoll W, Wegner G. Macromolecules 1995;28: 1214–20.
[35] Schmitt F-J, Yoshizawa H, Schmidt A, Duda G, Knoll W, Wegner G, et al. Macromolecules 1995;28:3401–10.
[36] Schmitt F-J, Müller M. Thin Solid Films 1997;310:138–47.
[37] Riou SA, Chien BT, Hsu SL, Stidham HD. J Polym Sci B Polym Phys 1997;35:2843–55.
[38] Mabuchi M, Ito S, Yamamoto M, Miyamoto T, Schmidt A, Knoll W. Macromolecules 1998;31:8802–8.
[39] Mabuchi M, Kobata S, Ito S, Yamamoto M, Schmidt A, Knoll W. Langmuir 1998;14:7260–6.
[40] Marsh D, Müller M, Schmitt F-J. Biophys J 2000;78:2499–510.
[41] Duda G, Wegner G. Makromol Chem Rapid Commun 1988;9:495–501.
[42] Yoshida M, Mitsui S, Nagoshi M, Kobayashi N, Hirohashi R. Synth Met 1999;102:1587–8.
[43] Itoh H, Ishii T, Satoh T. Eur. Pat. Appl. 232113; 1987.
[44] Hickel W, Duda G, Wegner G, Knoll W. Makromol Chem Rapid Commun 1989;10:353–9.
[45] Wasserman D, Garber JD, Meigs FM. U.S. Patent 3.285.953; 1966.
[46] Cornille F, Copier J-L, Senet J-P, Robin Y. Eur. Pat. Appl. 1201659; 2002.
[47] Wilder R, Mobashery S. J Org Chem 1992;57:2755–6.
[48] James MA, Voogt FC, Niesen L, Rogojanu OC, Hibma T. Surf Sci 1998;402–404:332–6.
[49] Sohling U, Schouten AJ. Langmuir 1996;12:3912–9.
[50] Miyazawa TJ. Chem Phys 1960;32:1647–52.
[51] Fasman GD, editor. Poly-α-amino acids: protein models for conformational studies. New York: Marcel Dekker, Inc.; 1967. 161–162, 196–201, 303–306, 503–519.
[52] Kricheldorf HR, Müller D, Förster H. Polym Bull 1982;8:487–94.
[53] Poche DS, Daly WH, Russo PS. Macromolecules 1995;28:6745–53.
[54] Uchida S, Oohori T, Tanaka T, Suzuki M, Shirai H. Macromol Chem Phys 1999;200:2645–50.
[55] Chang YC, Frank CW. Macromol Symp 1997;118:641–6.
[56] Komoto T, Kim KY, Kawai T. Makromol Chem 1978;179:373–85.
[57] Bhaw-Luximon A, Jhurry D, Belleney J, Goury V. Macromolecules 2003;36:977–82.
[58] Shoji A, Ozaki T, Fujito T, Deguchi K, Ando S, Ando I. J Am Chem Soc 1990;112:4693–7.
[59] Mitchell JC, Woodward AE, Doty P. J Am Chem Soc 1957;79:3955–60.
[60] Blout ER, de Loze C, Bloom SM, Fasman GD. J Am Chem Soc 1960;82:3787–9.
[61] Goodman M, Schmitt EE, Yphantis D. J Am Chem Soc 1960;82:3483–4.
[62] Goodman M, Schmitt EE, Yphantis D. J Am Chem Soc 1962;84:1288–96.
[63] Kricheldorf HR, Müller D, Stulz J. Makromol Chem 1983;184:1407–21.
[64] Kricheldorf HR. In: Penczek S, editor. Models of biopolymers by ring-opening polymerization. Boca Raton: CRC Press Inc; 1990 [Chapter 1].
[65] Blout ER, Karlson RH. J Am Chem Soc 1956;78:941–6.
[66] Doty P, Bradbury JH, Holtzer AM. J Am Chem Soc 1956;78:947–54.
[67] Doty P, Holtzer AM, Bradbury JH, Blout ER. J Am Chem Soc 1954;76:4493–4.
[68] Kricheldorf HR, von Lossow C, Schwarz G. Macromol Chem Phys 2004;205:918–24.
[69] Temyanko E, Russo PS, Ricks H. Macromolecules 2001;34:582–6.
[70] Block H. Poly(γ-benzyl-l-glutamate) and other glutamic acid containing polymers. New York: Gordon and Breach Publishers; 1983.
[71] Vayaboury W, Giani O, Cottet H, Deratani A, Schué F. Macromol Rapid Comm 2004;25:1221–4.
[72] Reda T, Hermel H, Höltje H-D. Langmuir 1996;12:6452–8.
[73] Fukuto M, Heilmann RK, Pershan PS, Yu SM, Griffiths JA, Tirrell DA. J Chem Phys 1999;111:9761–77.
[74] Gillgren H, Stenstam A, Ardhammar M, Nordén B, Sparr E, Ulvenlund S. Langmuir 2002;18:462–9.
[75] Zhukina EB, Birshtein TM, Borisov OV. Macromolecules 1995;28:1491–9.
[76] Stanley CB, Strey HH. Biophys J 2008;94:4427–34.
[77] Takekiyo T, Yoshimura Y, Okuno A, Shimizu A, Kato M, Taniguchi Y. Conf Ser. J Phys 2008;121:042003.
[78] Wang Y, Chang YC. Macromolecules 2003;36:6503–10.
[79] Matsushima N, Hikichi K, Tsutsumi A, Kaneko M. Polym J 1975;7:44–9.